Pergamon

Int. J. Heat Mass Transfer. Vol. 40, No. 14, pp. 3323–3334, 1997

Printed in Great Britain
0017–9310/97 $17.00+0.00

PII: S0017-9310(96)00379-1

Three-dimensional natural convective flow in a vertical annulus with longitudinal fins

RANGANATHAN KUMAR†
Clemson University, Clemson, SC 29631, U.S.A.

(*Received* 18 *January* 1996 *and in final form* 5 *November* 1996)

Abstract—Numerical results of heat transfer rates and flow fields in a vertical annulus with longitudinal fins for various parameters [Rayleigh number ($10^3 \leqslant Ra \leqslant 10^6$), radius ratio ($1 \leqslant \kappa \leqslant 5$), fin ratio $0.25 \leqslant FR \leqslant 0.75$, number of fins, and fin thickness angle ($\delta = 2°$ or 6°)] have been obtained. Placing fins of fin ratio 0.5 and fin thickness angle 6° on the inner cylinder of an annulus with radius ratio 2 increases the heat transfer by as much as 70%. For fixed Rayleigh number, radius ratio, aspect ratio, fin ratio and fin thickness angle, the heat transfer rate is maximum for a specific number of fins. The heat transfer rates increase as the fin ratio and radius ratio increase. In addition, the heat transfer rates decrease if the aspect ratio and the fin thickness angle increase. The maximum Nusselt number and optimum number of fins have been obtained as functions of various parameters. Heat transfer correlations have been provided in the range of the parameters considered. © 1997 Elsevier Science Ltd.

INTRODUCTION

Spent nuclear fuel is usually stored in casks that have inner and outer metallic shells. The shells are sealed at the top and bottom. The radioactivity of the spent nuclear fuel in the inner cylinder causes heating of the inner surface of the cask. The maximum amount of spent fuel that can be stored in the cask depends on the effectiveness of heat removal from the inner surface, and the design and properties of the cask material itself. The dominant mode of heat removal from the inner surface to the outer surface is natural convection of air in the cask. Heat transfer is considerably enhanced by having longitudinal fins on the inner surface. Therefore, for the efficient design of these casks with longitudinal fins, the determination of the heat transfer coefficients and flow pattern is necessary. The complexity of the geometry requires a three-dimensional analysis of both the flow and the heat transfer. The aspect ratio (height/annular gap width) of the cask is typically 2.5, with an inner radius of 1 in. The temperature difference between the inner and the outer cylinder is around 100 K. The Rayleigh number is of the order of 10^8. Therefore, the flow in the cask is likely to be turbulent. However, the benchmark laminar solution for finned annuli has not been established, and the current work attempts to do so.

In general, the literature on finned enclosures deals with square cavities, and not cylindrical annuli. Starner and McManus [1] experimentally investigated free convection heat transfer from a rectangular fin array. They studied the effects of orientation of the base plate, fin height, and fin spacing on the average heat transfer coefficients. The experiments with vertical fin arrays produced heat transfer results which fell 1–30% below those of similarly spaced parallel plates reported by Elenbaas [2]. Fitzroy [3] obtained a correlation for optimum spacing of a set of vertical fins, and showed that the optimum spacing decreased as the temperature difference between the surface and the ambient air increased.

Heat transfer results have indicated that the fin thickness could not be neglected in optimizing the total array heat transfer, as it influences both the efficiency of individual fins and the number of fins (Bar-Cohen [4], Tanaka *et al.* [5], and Tolpadi and Kuehn [6]). In this group of researchers, Tolpadi and Kuehn's [6] work involved a horizontal heated cylinder with a conducting transverse circular fin array. Karki and Patankar [7] did a numerical study of laminar natural convection in a vertical shrouded fin array, in which the flow is induced from surroundings by the chimney effect. Scozia and Frederick [8] obtained numerical solutions in a differentially heated slender cavity with transverse conduction fins on the cold wall.

Many studies have been done for different types of fin arrays, but, to the knowledge of the present author, no experimental or numerical investigation has been made to determine the effect of longitudinal fin arrays in a vertical annulus or cavity. The current paper focuses on the annular space enclosed between two

† Current address: Knolls Atomic Power Laboratory, Schenectady, NY 12301, U.S.A.

NOMENCLATURE

A	aspect ratio (H/L)
FR	fin ratio [fin width/gap width (L_f/L)]
H	height of annulus [m]
k_a	thermal conductivity of air
k_s	thermal conductivity of fin material
k	thermal conductivity ratio (k_s/k_a)
L	annulus gap width [m]
L_f	fin width [m]
n	number of fins
Nu	local Nusselt number ($\partial\tau/\partial R$)
$\overline{Nu}_i$	average Nusselt number for inner cylinder [$(Q_i/\Delta TA_i)(L/k_a)$]
$\overline{Nu}_o$	average Nusselt number for outer cylinder [$(Q_i/\Delta TA_o)(L/k_a)$]
$\overline{Nu}_{max}$	maximum $\overline{Nu}_i$ at optimum number of fins
P	non-dimensional pressure [$p'/(\rho\alpha^2/L^2)$]
Pr	Prandtl number
Q	heat transfer rate [W m^{-2}]
r	radial coordinate [m]
R	radial co-ordinate non-dimensionalized by L
R^*	$(R-R_i)/(R_o-R_i)$
Ra	Rayleigh number [$(g\beta\Delta TL^3)/\nu\alpha$]
T	temperature [°C]
V	non-dimensional velocity
Z	non-dimensional vertical coordinate.

Greek symbols

α	thermal diffusivity [m^2 s^{-1}]
Γ	diffusion coefficient in the discretized equation
δ	1/2 (fin thickness angle)
θ	azimuthal co-ordinate
Θ	angle between the centers of two adjacent fins
Θ_{opt}	optimum angle between fins for maximum heat transfer
κ	radius ratio (R_o/R_i)
ν	kinematic viscosity [m^2 s^{-1}]
ρ	density [kg m^{-3}]
τ	non-dimensional temperature [$(T-T_o)/(T_i-T_o)$]
ϕ	dependent variable in the discretized equation.

Subscripts, superscripts and primes

$'$	dimensional quantity
i	inner
o	outer
r	reference.

coaxial vertical circular cylinders with longitudinal fins and horizontal plates at the top and bottom. The effect of the following parameters on heat transfer and fluid flow will be investigated: Rayleigh number (Ra), fin angle (Θ), radius ratio (κ), and aspect ratio (A). Selected results have also been obtained for different fin thickness angles (δs), and fin ratios (FRs).

MATHEMATICAL FORMULATION AND SOLUTION PROCEDURE

The governing equations for the laminar motion of a Newtonian fluid are derived from the conservation laws of mass, momentum and energy. The flow is assumed to be steady. The Boussinesq approximation is used, i.e. the density is treated as a constant for all terms except the buoyancy term of the momentum equation in the vertical (Z) direction. The density difference term is rewritten as a function of the temperature only, given by $(\rho-\rho_r) = -\rho_r\beta(T-T_r)$ where β is the coefficient of volumetric expansion, and T is the temperature. The heat transfer is predominantly in the radial direction from the inner cylinder to the outer cylinder: therefore, the length scale is taken to be the gap width (L). The three velocity components are normalized by α/L, and the pressure by $\rho\alpha^2/L^2$. The non-dimensional governing equations are given as follows:

Continuity:

$$\frac{1}{R}\frac{\partial}{\partial R}(RV_R)+\frac{1}{R}\frac{\partial}{\partial\theta}(RV_\theta)+\frac{\partial V_z}{\partial Z}=0 \qquad (1)$$

R-*momentum*:

$$V_R\frac{\partial V_R}{\partial R}+\frac{V_\theta}{R}\frac{\partial V_R}{\partial\theta}+\frac{V_\theta^2}{R}+V_z\frac{\partial V_R}{\partial Z}=Pr\left[\frac{\partial}{\partial R}\left(\frac{1}{R}\frac{\partial}{\partial R}(RV_R)\right)+\frac{1}{R^2}\frac{\partial^2 V_R}{\partial\theta^2}-\frac{2}{R^2}\frac{\partial V_\theta}{\partial\theta}+\frac{\partial^2 V_R}{\partial Z^2}\right]-\frac{\partial P}{\partial R} \qquad (2)$$

θ-momentum:

$$V_R\frac{\partial V_\theta}{\partial R}+\frac{V_\theta}{R}\frac{\partial V_\theta}{\partial \theta}+\frac{V_R V_\theta}{R}+V_z\frac{\partial V_\theta}{\partial Z}=Pr\left[\frac{\partial}{\partial R}\left(\frac{1}{R}\frac{\partial}{\partial R}(RV_\theta)\right)+\frac{1}{R^2}\frac{\partial^2 V_\theta}{\partial \theta^2}+\frac{2}{R^2}\frac{\partial V_R}{\partial \theta}+\frac{\partial^2}{\partial Z^2}(V_\theta)\right]-\frac{1}{R}\frac{\partial P}{\partial \theta} \quad (3)$$

Z-momentum:

$$V_R\frac{\partial V_Z}{\partial R}+\frac{V_\theta}{R}\frac{\partial V_Z}{\partial \theta}+V_Z\frac{\partial V_Z}{\partial Z}=Pr\,Ra\,\tau+Pr\left[\frac{1}{R}\frac{\partial}{\partial R}\left(R\frac{\partial V_Z}{\partial R}\right)+\frac{1}{R^2}\frac{\partial^2 V_Z}{\theta^2}+\frac{\partial^2 V_Z}{\partial Z^2}\right]-\frac{\partial P}{\partial Z} \quad (4)$$

Energy:

$$V_R\frac{\partial \tau}{\partial R}+\frac{V_\theta}{R}\frac{\partial \tau}{\partial \theta}+V_Z\frac{\partial \tau}{\partial Z}=\frac{1}{R}\frac{\partial}{\partial R}\left(R\frac{\partial \tau}{\partial R}\right)+\frac{1}{R^2}\frac{\partial^2 \tau}{\partial \theta^2}+\frac{\mathrm{d}^2\tau}{\mathrm{d}Z^2}. \quad (5)$$

Boundary conditions

The flow domain is enclosed in the annular space between two coaxial vertical circular cylinders with longitudinal fins, and sealed top and bottom plates [Fig. 1]. The computational domain consists of a wedge, with both edges running through the middle of the fins in the θ-direction, the inner and the outer cylinder in the R-direction, and the top and the bottom adiabatic walls in the Z-direction. The inner and outer cylinders are maintained at constant temperatures (T_i and T_o, respectively), with $T_i > T_o$. Symmetry boundary conditions are imposed on the edges running through the middle of the fins. No slip boundary conditions are used for all the solid–fluid interfaces. The wedge angle is changed when the effect of the number of fins (n) is of interest. The top view of the computational domain is shown in Fig. 1.

Angular fins are used in the present model. The thickness of the fin increases in the radial direction. Usually, in practical applications, straight and parallel fins are used. The present model is good for short and thin fins representing straight fins. The normalized boundary conditions are

$$\theta=0 \quad \text{and} \quad \theta=\Theta: \quad \frac{\partial V_\theta}{\partial \theta}=\frac{\partial V_R}{\partial \theta}=\frac{\partial V_Z}{\partial \theta}=\frac{\partial \tau}{\partial \theta}=0 \quad (6)$$

$$Z=0 \quad \text{and} \quad Z=A: \quad V_\theta=V_R=V_Z=0; \quad \frac{\partial \tau}{\partial Z}=0 \quad (7)$$

$$R=\frac{r_i}{L}: \quad V_\theta=V_R=V_Z=0; \quad \tau=1 \quad (8)$$

$$R=\frac{r_i}{L}: \quad V_\theta=V_R=V_Z=0; \quad \tau=0. \quad (9)$$

Heat transfer results are the average values of the Nusselt number and the local value of the Nusselt number for each wall. The Nusselt number expressions are

$$\overline{Nu_i}=\frac{1}{2\pi R_i A}\int_0^{2\pi-2n\delta}\int_0^A \frac{\partial \tau}{\partial R}(R_i\,\mathrm{d}\theta\,\mathrm{d}Z)+\frac{k}{2\pi R_i A}\int_0^{2n\delta}\int_0^A \frac{\partial \tau}{\partial R}(R_i\,\mathrm{d}\theta\,\mathrm{d}Z) \quad (10)$$

$$Nu_0=\frac{1}{2\pi R_0 A}\int_0^{2\pi}\int_0^A \frac{\partial \tau}{\partial R}(R_0\,\mathrm{d}\theta\,\mathrm{d}Z) \quad (11)$$

where k is the ratio of the thermal conductivity of the fin material to that of air.

Numerical procedure

The governing equations were solved by using a computer code, PHOENICS, based on a control volume formulation [9]. The governing differential equations are integrated over the control volume surrounding a grid point. Piecewise profiles expressing the variation of the dependent variable (ϕ) between the grid points are used to evaluate the required integrals from the governing differential equations. PHOENICS provides solutions to a discretized version of the set of differential equations having the general form

$$\frac{\partial}{\partial t}(\rho\phi)+\nabla\cdot(\rho V\phi-\rho\Gamma_\phi\nabla\phi)=S_\phi. \quad (12)$$

The dependent variable (ϕ) stands for the temperature, velocity component, etc. Depending on these variables, an appropriate property will be assigned to the diffusion coefficient (Γ_ϕ), and the source term (S_ϕ). No slip velocity boundary condition at the solid–fluid interface and constant temperatures on the inner and outer cylinders are implemented through the source term (S_ϕ) in PHOENICS. Since there are no grid points on the boundary of the computational domain, the finite-difference equations are modified for those cells that have cell faces adjoining the boundaries of the computation domain. The interface between the solid and the fluid is treated like any other interface between two control volumes, with only the value of Γ_ϕ changing at the interface.

Under-relaxation is done as suggested by Patankar [9] and Van Doormaal [10]. All computations were made on a Sun Workstation Sparc 1. Convergence

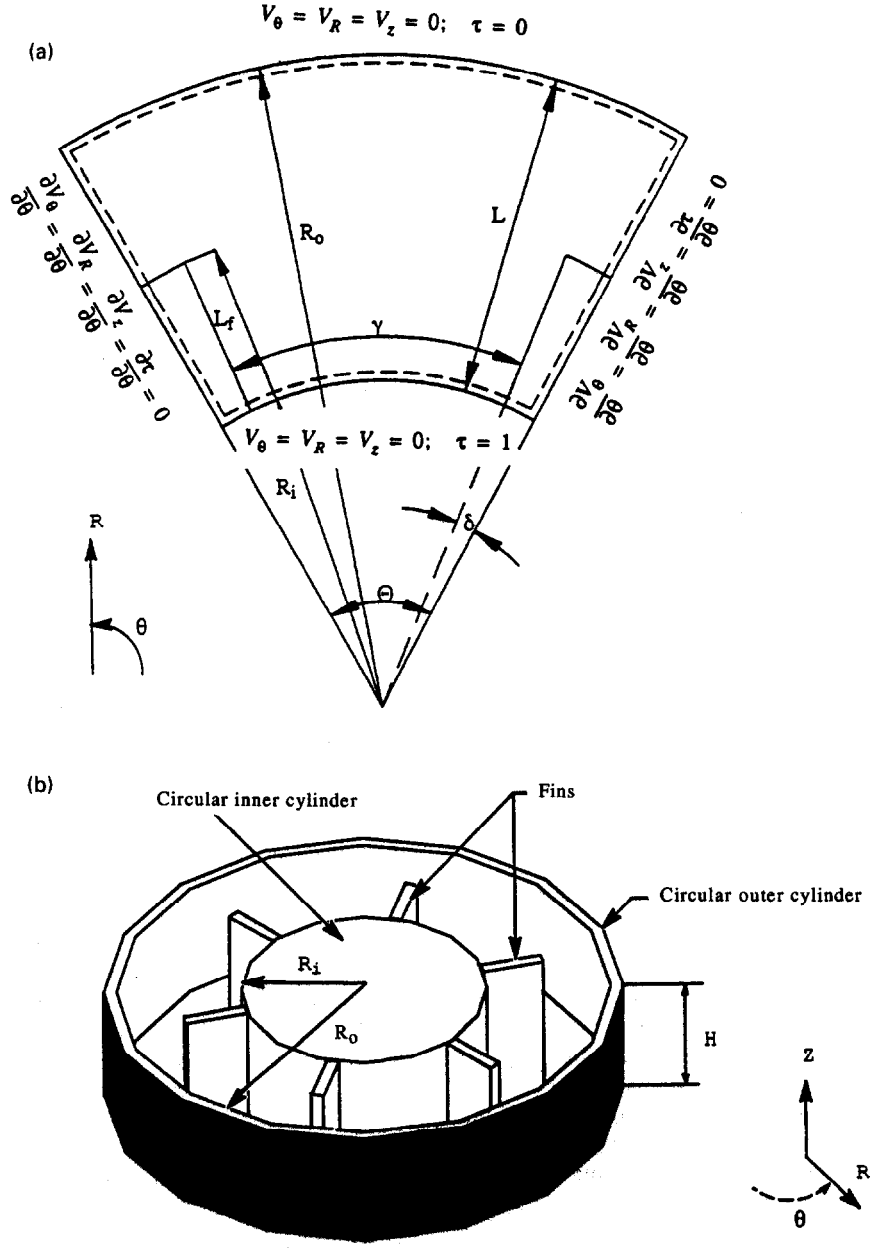

Fig. 1. (a) Top view of the computational domain; (b) flow geometry of the finned annulus.

criteria were set to ensure converged results for the mass and energy balances. For the mass balance, a solution was assumed to converge if the maximum mass imbalance was less than 0.01%. For the energy balance, iterations were continued until the maximum change in temperature at any node as a fraction of the maximum temperature in the domain was less than 0.1%. In addition, residuals of all variables were set to a typical value of 10^{-5}. Typically, 400–600 iterations were needed to get a converged solution. For higher Rayleigh numbers, twice as many iterations were needed to obtain convergence. A thorough study of grid-independent solutions was done. The number of grid points used was $26 \times 28 \times 72$ ($R \times \theta \times Z$) for most of the cases. Selectively, a coarser grid of $26 \times 8 \times 20$ was used for $\theta = 12°$ and $A = 1$. When this coarse grid was tested against the finer grid, heat transfer results varied by less than 1%. Finer grids than $26 \times 28 \times 72$ were tested for high aspect ratio cases, but the change in the results was insignificant. For the same geometric parameters, the converged solution obtained from lower Rayleigh numbers was used as the starting condition to run cases for higher Rayleigh numbers. The results also compared favorably with some benchmark results, as discussed in the next section.

Table 1. Comparison of $\overline{Nu_i}$ for vertical cavity and annulus

Ra	κ	$\overline{Nu_i}$ (current study)	$\overline{Nu_i}$ (refs. [11, 12])	% difference
1×10^4	1	2.256	2.242	0.62
1×10^5	1	4.526	4.523	0.07
1×10^3	2	1.600	1.572	1.75
1×10^4	2	3.105	3.305	6.10
1×10^5	2	6.107	6.268	2.60
2×10^5	2	7.464	7.600	1.80
1×10^3	5	2.681	2.550	4.90

Table 2. Comparison of $\overline{Nu_i}$ for annulus

Ra	κ	$\overline{Nu_i}$ (current study)	$\overline{Nu_i}$ (ref. [12])	% difference
1×10^4	1.33	1.451	1.421	2.09
4×10^4	1.33	2.206	2.09	5.26
1×10^5	1.33	2.857	2.696	5.62

RESULTS AND DISCUSSION

Natural convection of air is studied numerically in a vertical annulus with longitudinal fins. The inner wall is maintained at a constant temperature (T_i), and the outer wall at a constant but lower temperature (T_o). The effects of κ, A, Ra, δ and number of fins on the inner cylinder on the heat transfer and fluid flow results are discussed in this section.

Validation of numerical results

The numerical model was validated by comparing different limited cases with available results in the literature. The model was used to validate results for natural convection in a vertical cavity. The overall local Nusselt numbers and maximum velocity values were compared with the benchmark solution of de Vahl Davis [11] for a vertical square cavity, and of Kumar and Kalam [12] for vertical annuli. Nusselt numbers are in very good agreement, as shown in Table 1. A κ of 1 indicates a square cavity. For a δ of 6° and an FR of 0.5, two-dimensional heat transfer results can be obtained by considering no fins or 30 fins (Θ) = 12°. Flow in the annulus with no fins would give results for a κ of 2. Flow in the annulus with 30 fins, $FR = 0.5$ and $\delta = 6°$ would give results for a κ of 1.33. Results obtained for $k = 2$ and no fins are given in Table 1. Results for $\kappa = 1.33$ and 30 fins are given in Table 2. These results were generated because no experimental results for finned annuli were available for comparison.

Velocity field

Velocity vectors for $Ra = 10^4$, 10^5 and 10^6, $\Theta = 30°$ and $\kappa = 1.2$ are shown in Fig. 2. For clarity, some of the velocity vectors are removed from Fig. 2. For $Ra = 10^4$, there is only one cell because of lower convective activity between the fins. In between the fins

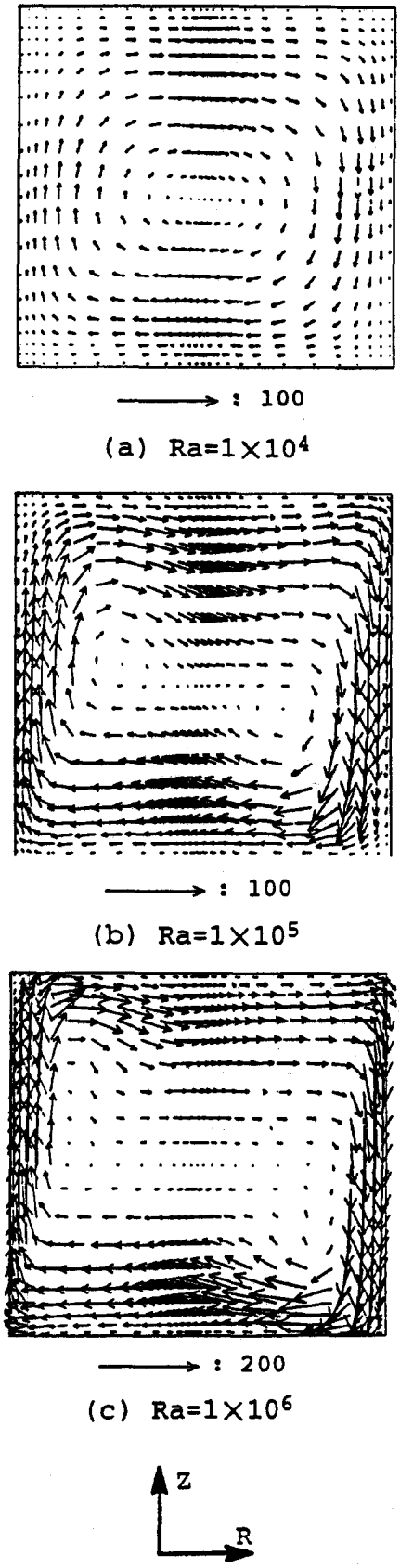

Fig. 2. Velocity vectors at $\theta/\Theta = 0.5$ for $\Theta = 30°$, $\kappa = 1.2$, $FR = 0.5$, $\delta = 6°$ and $A = 1$.

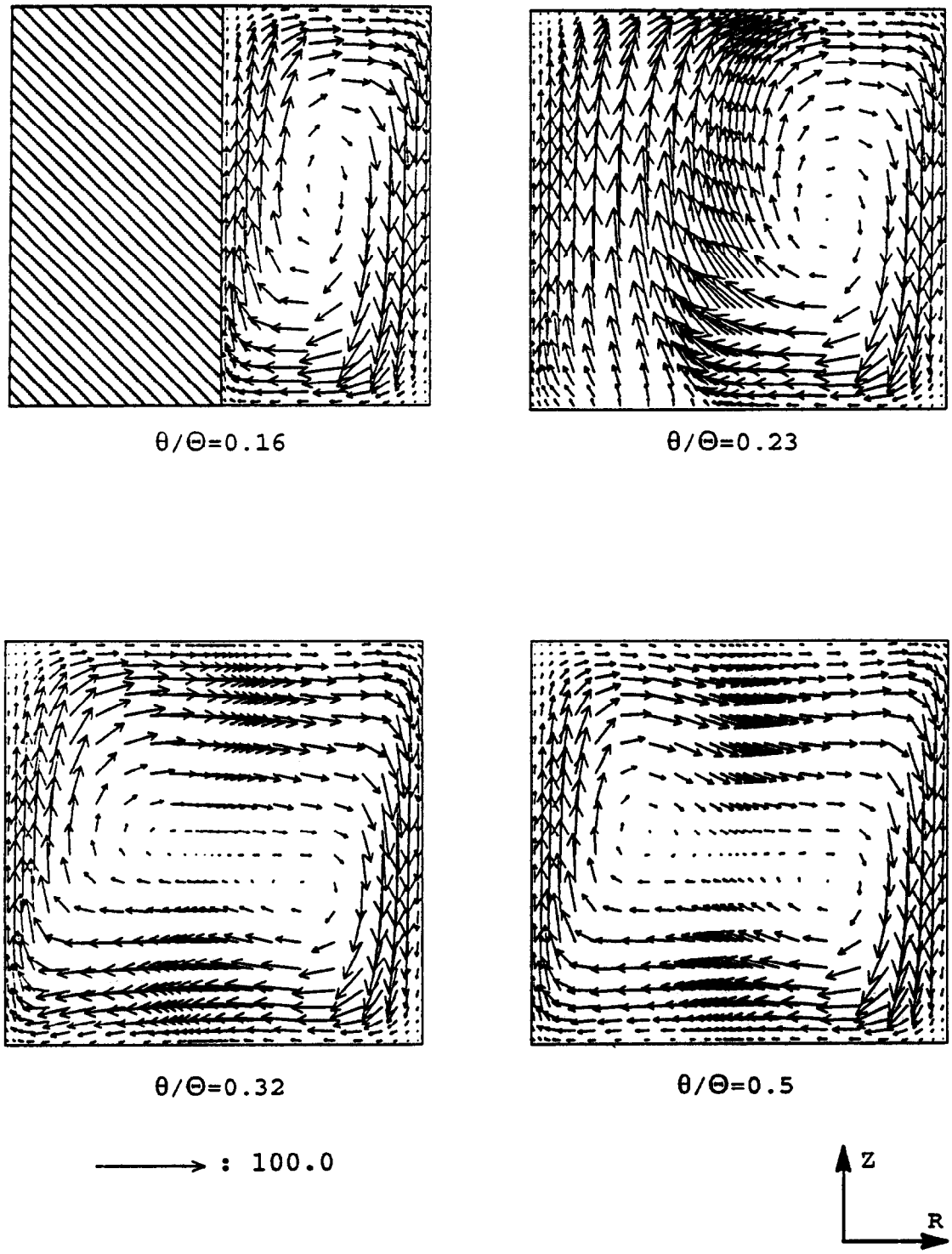

Fig. 3. Velocity vectors at different circumferential locations for $Ra = 10^5$, $\Theta = 30°$, $\kappa = 1.2$, $FR = 0.5$, $A = 1$ and $\delta = 6°$.

(i.e. $\theta/\Theta = 0.5$), as Ra is increased, two cells begin to appear, and, at 10^6, two counter-rotating cells can be clearly seen. In Fig. 3, formation of the cell at different circumferential locations is shown for $Ra = 10^5$. The two cells that appear at the central location merge into a single cell closer to the fin.

Vertical, radial and circumferential velocity profiles for the case of $\Theta = 30°$, $\kappa = 1.2$, $FR = 0.5$ and $Ra = 10^5$ are given in Fig. 4. As expected, the vertical velocities close to the cylinder walls are dominant at the central circumferential locations [Fig. 4(a) and (b)]. In the mid-portion of the cylinder

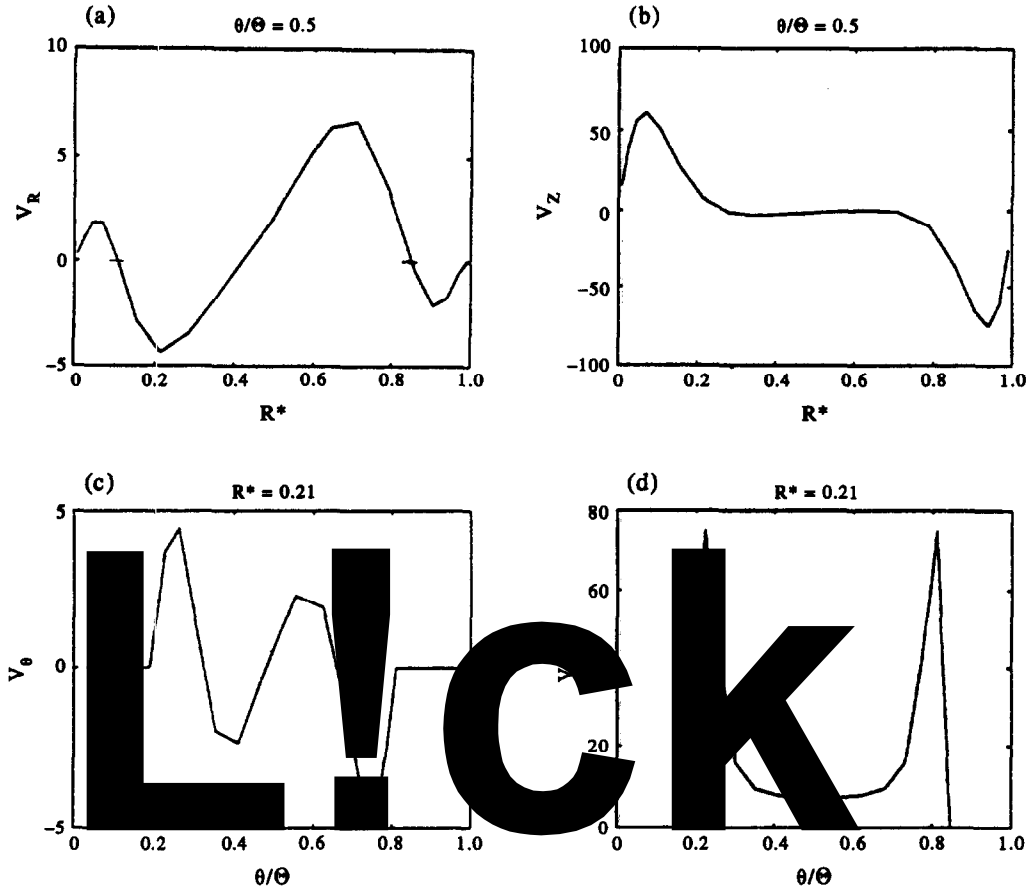

Fig. 4. Velocity distribution at $Z = 0.5$ for $\Theta = 30°$, $\kappa = 1.2$, $FR = 0.5$, $\delta = 6°$, and $A = 1$.

$(0.3 < R < 0.7)$, the axial velocity is nearly zero. The flatness of the V_Z-profile, and the small and nearly anti-symmetric radial and tangential velocity profiles, indicate that secondary cells are being formed. The V_θ-profile shows flow symmetry about the vertical plane passing through $\theta/\Theta = 0.5$. This symmetry was seen for all *Ra*s considered for $\kappa = 1.2$. Figure 4(d) shows the vertical velocity symmetry about the azimuthal direction. For $Ra = 10^5$, Fig. 5 shows the curvature effect of the flow field. As the diameter ratio is increased from 1.2 to 5.0, secondary circulation disappears; only one cell is present, and the center of rotation moves slightly towards the outer cylinder.

Effect of the number of fins

The number of fins (n) on the inner cylinder can be optimized to achieve maximum heat transfer. As Θ is increased (or, alternatively, as n is decreased), the total surface area on the inner cylinder decreases, and the temperature gradient increases. Because of these opposing effects, there exists an optimum fin angle (Θ_{opt}) for maximum heat transfer. The effect of interaction between the fins on the circumferential temperature profile can be seen in Fig. 6. The profiles are given at three radial locations (between the fins, close to the tips, and close to the outer cylinder) and three vertical locations. As Θ is decreased, the temperature profiles flatten due to a strong thermal interaction between the fins and the restricted flow. At $R = 0.28$, $Z = 0.25$, 0.5 and 0.75, the temperature gradient at the fin surface decreases in the circumferential direction as Θ decreases. For $\Theta = 15°$, heat transfer from the fin surface is insignificant. This effect is seen at $R = 0.28$ and 0.5. At $R = 0.71$, the temperature profile in the circumferential direction is more or less uniform for all Θ, due to the absence of a solid surface.

Figure 7 gives the heat transfer on the inner cylinder as a function of Θ for two different *Ra* and two different δs. The Θ_{opt} for $\delta = 6°$ decreases from 30 to 24° when *Ra* is increased from 10^4 to 10^5. The reason may be given as follows. As *Ra* is increased for the same Θ, the flow becomes more buoyant between the fins. This increases the fluid velocity, reducing the thermal interaction between the fins in the circumferential direction. This, in turn, increases the temperature gradient. Therefore, the fins can be brought closer (i.e. Θ can be decreased), without reducing the heat transfer until the thermal interaction between the fins becomes appreciable enough to decrease the temperature gradient. For example, by decreasing Θ to 24° (i.e. by increasing n), the total surface area is increased, thereby optimizing the heat transferred. Therefore, as *Ra* increases, Θ_{opt} decreases.

It is also seen from Fig. 7 that, as δ is decreased

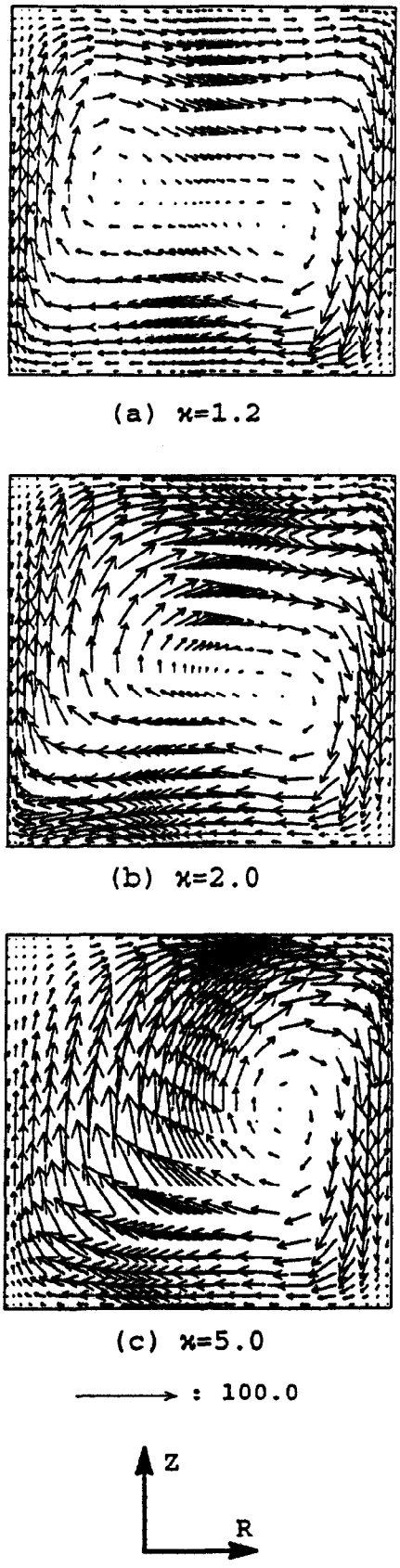

Fig. 5. Velocity vectors at $\theta/\Theta = 0.5$ for $\Theta = 30°$, $Ra = 10^5$, $FR = 0.5$, $\delta = 6°$ and $A = 1$.

from 6° to 2°, maximum heat transfer is achieved (by 8% for $Ra = 10^5$) by increasing the number of fins, i.e. Θ_{opt} decreases when δ is decreased. For $\Theta < \Theta_{opt}$, $\overline{Nu}_i$ increases as δ is decreased from 6 to 2° for a given Θ. beyond Θ_{opt}, the opposite effect is seen.

The observations from Fig. 7 may be summarized as follows: when the fin thickness is reduced, with more fins on the inner cylinder, further enhancement of heat transfer is achieved. By merely decreasing δ, one cannot obtain a high heat transfer for the same number of fins. This mechanism can be explained and further corroborated using radial temperature profiles at different circumferential location given in Fig. 8. The temperature gradient is higher at the fin tip surface than at the surface of the inner cylinder. The fluid enclosed between the fins and the inner cylinder is at a higher temperature than the fluid near the fin tip. Therefore, the fluid near the fin tip is at a higher temperature gradient, increasing the effective local heat transfer rate. Any reduction in the fin thickness would cause a reduction in local heat transfer at the fin tip. However, the spacing between the fins would increase for the same Θ, and this would increase the local temperature gradient in the circumferential direction. Thus, a decrease in δ causes a decrease in heat transfer at the fin tip, and an increase elsewhere on the fin surface. The overall heat transfer ($\overline{Nu}_i$) will increase or decrease depending on Θ. In external flows with circular fin arrays, Tolpadi and Kuehn [6] found that the heat transfer increases as the fin thickness decreases.

Effect of length of fin

An increase in the width of the fin increases the heat transfer from the inner cylinder, because a greater surface area is available for heat transfer from the fins. As shown in Fig. 9, $\overline{Nu}_{max}$ increases as FR is increased. The optimum angle for maximum local heat transfer (Θ_{opt}) increases very slightly as FR increases, but the increase in $\overline{Nu}_{max}$ is appreciable when FR is increased from 0.25 to 0.5. Both quantities are linear functions of Ra. An FR of 0.5 has been chosen for the remainder of the cases considered to explore the effects of differential geometrical parameters.

Effect of radius ratio

As κ is increased for the same FR, total heat transfer from the inner cylinder increases because a greater surface area is available. The variation of $\overline{Nu}_i$ with κ for different Ra at $\Theta = 30°$ is shown in Fig. 10. By decreasing the temperature gradient and increasing the surface area, Θ_{opt} can be increased for the same Ra, δ and A. The increase in Θ_{opt} and $\overline{Nu}_{max}$ for various κs and their linear variation with Ra on a logarithmic scale are shown in Fig. 11. In Fig. 11, the results for $\kappa = 1$ and $\kappa = 2$ can be compared directly since the ratio of fin width to gap width is the same. Direct comparisons of $\kappa = 1$ and κs other than 2 may not be made. $\overline{Nu}_{max}$ increases with Ra, and, at $Ra = 10^5$, it increases by almost 50% when κ is increased from 1

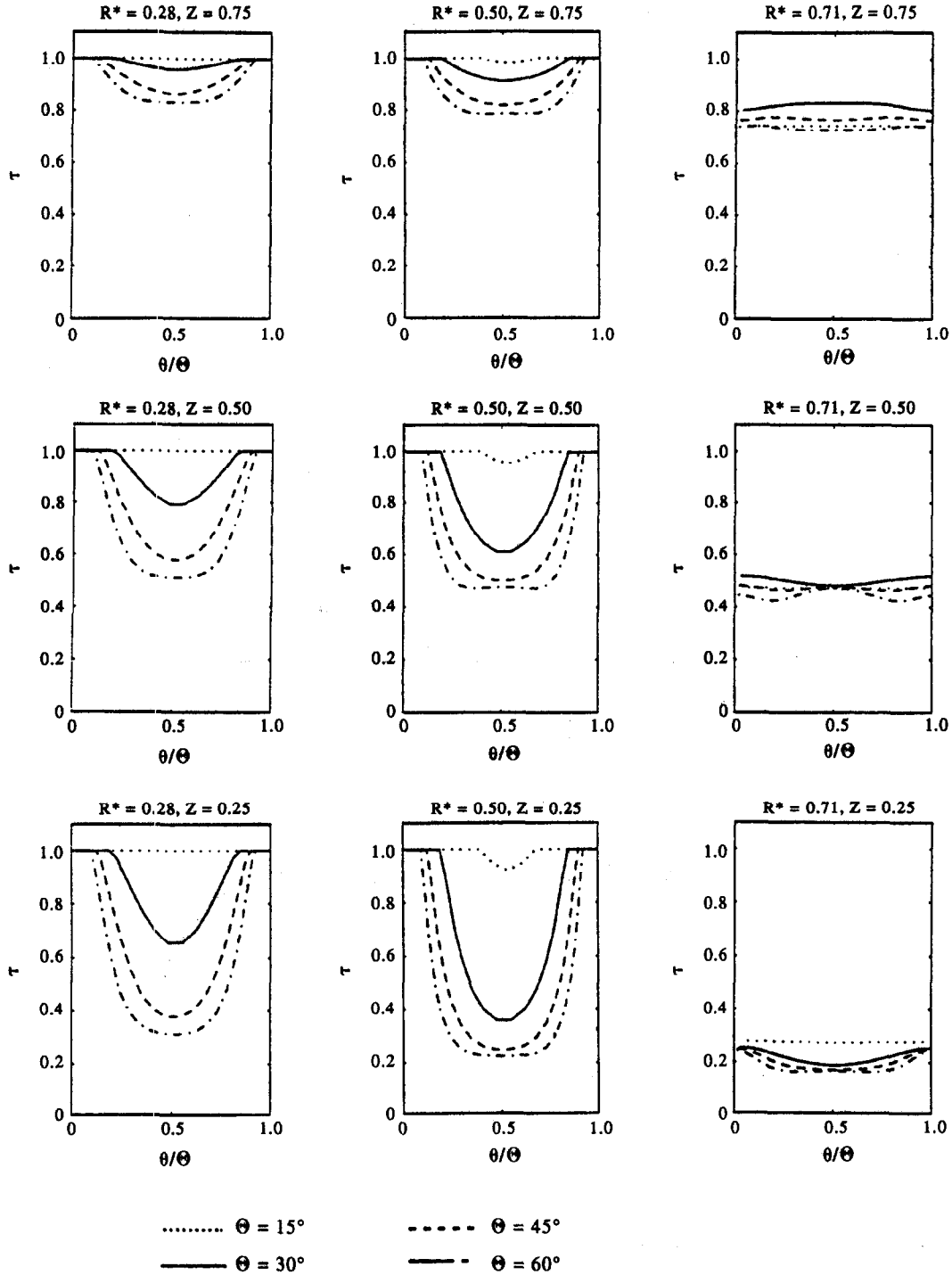

Fig. 6. Circumferential temperature profiles, showing the interactions between the fins for different fin angles: $Ra = 10^4$, $\kappa = 2$, $\delta = 6°$, $A = 1$ and $FR = 0.5$.

to 2, keeping all other parameters constant. For a given κ, Θ_{opt} decreases with Ra, and, when κ is increased, Θ_{opt} also increases. Comparing $\kappa = 1$ and $\kappa = 2$ again, the results show that Θ_{opt} is higher for $\kappa = 1$ at all Ra.

Effect of aspect ratio

The thermal boundary layer thickness on the inner cylinder increases in the vertical direction, thereby decreasing the temperature gradient. Therefore, Nu decreases in the increasing vertical direction. As A

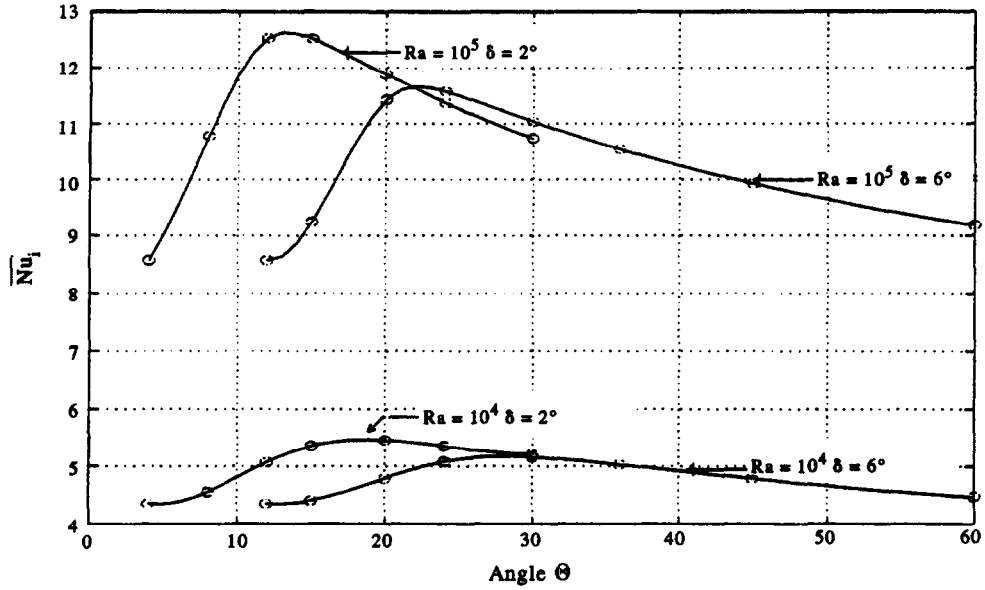

Fig. 7. $\overline{Nu}_i$ for different Θs in the convection regime: $\kappa = 2$, $FR = 0.5$ and $A = 1$.

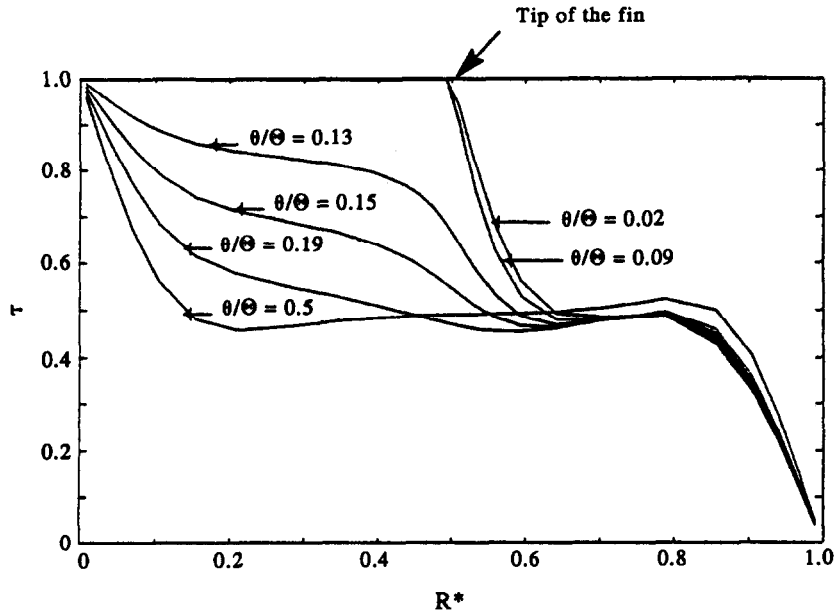

Fig. 8. Temperature profiles at different circumferential locations: $Z = 0.5$ for $Ra = 10^5$, $\Theta = 60°$, $\kappa = 2$, $FR = 0.5$, $\delta = 6°$ and $A = 1$.

increases, the average Nusselt number should also decrease. The variation of Θ_{opt} and $\overline{Nu}_{max}$ with Ra is shown in Fig. 12. $\overline{Nu}_{max}$ decreases with increasing A. If A is reduced from 5 to 1, $\overline{Nu}_{max}$ increases by 35% at $Ra = 10^5$. Since the average temperature gradient decreases with increasing A, Θ_{opt} increases as shown in Fig. 12. Although Θ_{opt} varies between A values of 1 and 2, the magnitude of $\overline{Nu}_{max}$ itself does not change significantly, especially at lower Ras.

Correlations

Correlations for the determination of $\overline{Nu}_{max}$ and Θ_{opt} as functions of Ra, A and κ for $\delta = 6°$ and $FR = 0.5$ are provided. Since the variation of $\overline{Nu}_{max}$ and Θ_{opt} with Ra and is linear in the logarithmic scale, the general form of the correlations are

$$\overline{Nu}_{max} = c\, Ra^l k^m \tag{13}$$

$$\Theta_{opt} = c\, Ra^q k^r. \tag{14}$$

From the numerical data obtained, the values of the constants in equations (13) and (14) are given in Table 3. In the correlation given above, A is not included directly. This is because l, m and r appear to be functions of A. Nearly 200 cases were run for various geometric parameters and Ras ($10^4 \leqslant Ra \leqslant 10^6$,

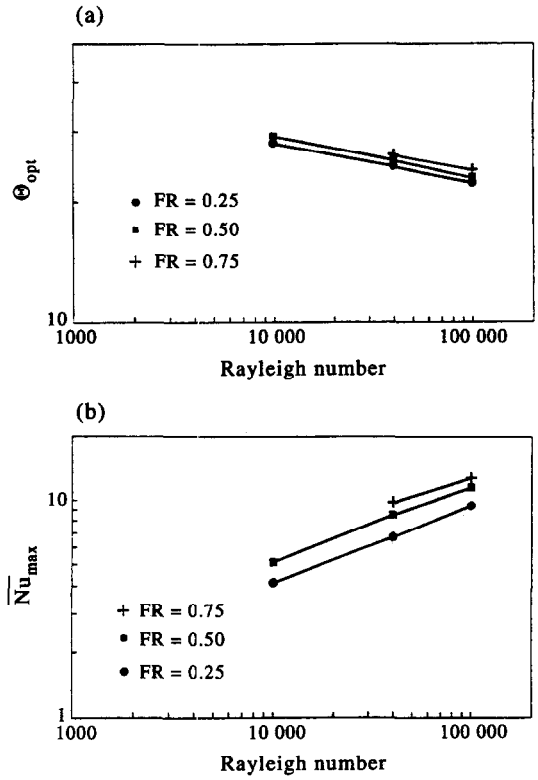

Fig. 9. Effect of Ra for different FRs ($\kappa = 2$, $\delta = 6°$ and $A = 1$) on Θ_{opt} (a), and $\overline{Nu}_{max}$ (b).

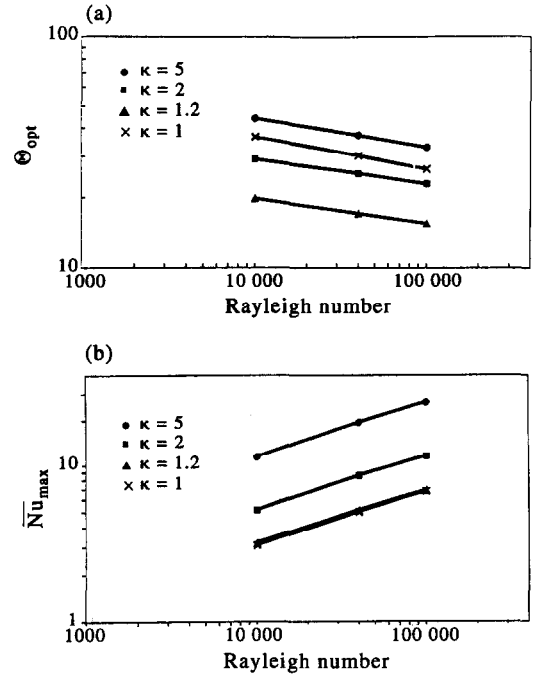

Fig. 11. Effect of Ra on Θ_{opt} (a) and $\overline{Nu}_{max}$ (b) for different κs and $A = 1$.

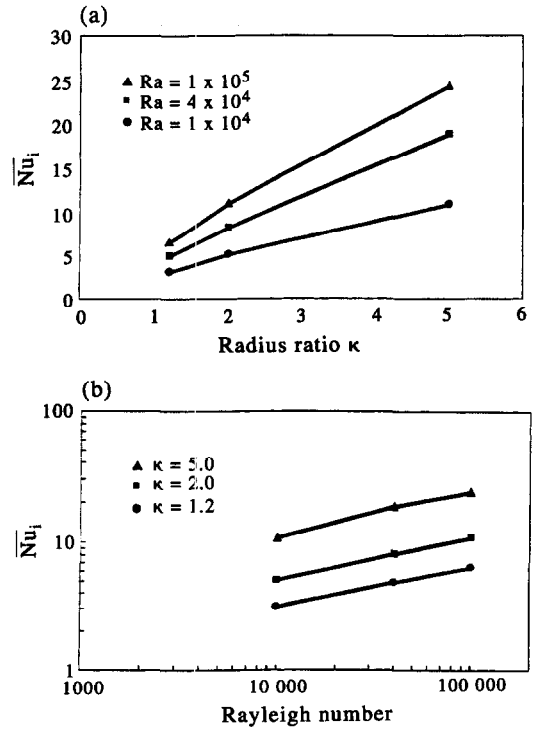

Fig. 10. $\overline{Nu}_i$ variation for $\Theta = 30°$, $FR = 0.5$, $\delta = 6°$ and $A = 1$.

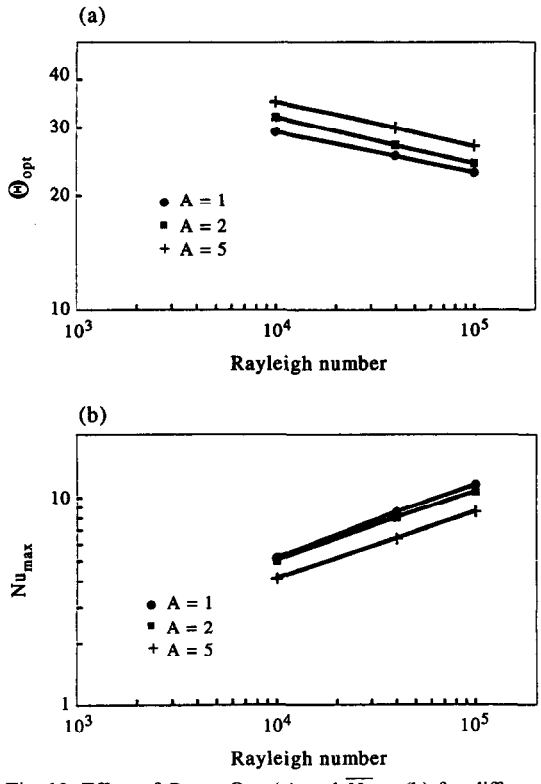

Fig. 12. Effect of Ra on Θ_{opt} (a) and $\overline{Nu}_{max}$ (b) for different As: $\delta = 6°$, $\kappa = 2$ and $FR = 0.5$.

Table 3. Correlation constants

As	C	l	m	D	q	r
1	0.109	0.35	0.89	55.6	−0.115	0.535
2	0.121	0.333	0.882	57.7	−0.115	0.563
5	0.123	0.316	0.865	59.9	−0.115	0.610

$1 \leqslant \kappa \leqslant 5$, $1 \leqslant A \leqslant 5$, $\delta = 6°$, $FR = 0.5$). The maximum and rms error for the $\overline{Nu}_{max}$ correlation are 6 and 0.6%, respectively. The maximum and rms error for the Θ_{opt} correlation are 11 and 2.6%. In a problem where a number of parameters play an important role, it is rather difficult to obtain exponents in correlations as functions of geometrical parameters, as done for unfinned vertical annuli by Kumar and Kalam [12]. From a practical standpoint, the correlation for $A = 1$ would be more useful since it has been already shown that $\overline{Nu}_{max}$ is highest for $A = 1$ among the three As considered. In other words, given a certain amount of spent nuclear waste to store, it is advisable to use many short cylinders rather than one long cylinder.

SUMMARY AND CONCLUSIONS

A numerical solution to three-dimensional natural convective flow in a vertical annulus with longitudinal fins has been obtained using the code PHOENICS. The numerical results were validated with available results in the literature for the case of a vertical annulus without longitudinal fins. Based on the current results for the finned annuli, the following conclusions may be made:

(1) The heat transfer rate from the inner cylinder is found to be maximum for a specific number of fins. The maximum heat transfer and the optimum number of fins changes with Ra, κ, A, δ and n.
(2) The temperature and velocity fields show a strong dependence on various geometric parameters. The colder fluid is confined to a large region near the base of the annulus, and this region increased in size as κ increased. The center of rotation shifted towards the outer wall as κ increased. The secondary cells observed in the case of lower κ completely vanish for higher κ.
(3) $\overline{Nu}_{max}$ and Θ_{opt} increase with κ. By increasing κ from 1 (square cavity) to 5, the maximum heat transfer rate can be increased significantly.
(4) Heat transfer rates decreased as A increased beyond 1. Therefore, shorter cylinders are recommended for waste storage.
(5) Correlations have been obtained for $\overline{Nu}_{max}$ and Θ_{opt} as functions of Ra and κ. Values of the exponents are provided for three different As.

It is recommended that modified correlations be obtained in the future using turbulence models and variable property effects. Low A cases may present interesting and useful results as well.

Acknowledgement—The author expresses gratitude to Manish Narain who ran the numerical code, and obtained all the results.

REFERENCES

1. Starner, K. E. and McManus, H. N., Jr., An experimental investigation of free convection heat transfer from rectangular fin arrays. *ASME Journal of Heat Transfer*, 1963, **85**, 273–278.
2. Elenbaas, W., Heat dissipation of parallel plates by free convection. *Physica*, 1948, **9**, 1–28.
3. Fitzroy, N. D., Optimum spacing of fins by free convection. *ASME Journal of Heat Transfer*, 1971, **93**, 462–463.
4. Bar-Cohen, A., Fin thickness for an optimized natural convection array of rectangular fins. *ASME Journal of Heat Transfer*, 1979, **101**, 564–566.
5. Tanaka, S., Yoshida, T. and Kunitomo, T., Optimization and heat transfer for a vertical fin array on isothermal and non-isothermal plane surfaces with combined natural convection and radiation. *Heat Transfer—Japanese Research*, 1987, **16**, 91–112.
6. Tolpadi, A. K. and Kuehn, T. H., Computation of conjugate three-dimensional natural convection heat transfer from a transversely finned horizontal cylinder. *Numerical Heat Transfer, Part A*, 1989, **16**, 1–13.
7. Karki, K. C. and Patankar, S. V., Cooling of a vertical shrouded fin array by natural convection: a numerical study. *ASME Journal of Heat Transfer*, 1987, **109**, 671–676.
8. Scozia, R. and Frederick, R. L., Natural convection in slender cavities with multiple fins attached to an active wall. *Numerical Heat Transfer, Part A*, 1991, **20**, 127–158.
9. Patankar, S. V., *Numerical Heat Transfer and Fluid Flow*. Hemisphere, New York, 1980.
10. Van Doormaal, J. P. and Raithby, G. D., Enhancement of SIMPLE method for predicting incompressible fluid flows. *Numerical Heat Transfer*, 1984, **7**, 147–163.
11. de Vahl Davis, G., Natural convection of air in a square cavity: a bench mark numerical solution. *International Journal of Numerical Methods in Fluids*, 1983, **3**, 249–264.
12. Kumar, R. and Kalam, M. A., Laminar thermal convection between vertical coaxial isothermal cylinders. *International Journal of Heat and Mass Transfer*, 1991, **34**, 513–524.